Submitted October 2002

A Comparison of Steel/Concrete and Glass Fiber Reinforced Polymers/Concrete Interface Testing by Guided Waves

by Won-Bae Na,* Tribikram Kundu† and Mohammad R. Ehsani†

ABSTRACT

Glass fiber reinforced polymer rods or bars are being used for reinforcing concrete structures. In comparison to conventional steel reinforcing bars, the glass fiber reinforced polymer bars are less likely to corrode when subjected to deicing materials and seawater. However, glass fiber reinforced polymers can be corroded due to chemical reactions that are different from the ones that corrode steel. This corrosion can deteriorate the glass fiber reinforced polymer/concrete interface and cause delamination or loss of bond, the most common secondary interface deterioration in reinforced concrete. Ultrasonic guided waves, because of their long distance testing capability, have been used for detecting delamination at the steel/concrete interface. In this paper, the possibility of developing similar guided wave testing techniques for testing glass fiber reinforced polymer/concrete interface delamination is investigated. Developing ultrasonic techniques for glass fiber reinforced polymer/concrete interface testing is more challenging because glass fiber reinforced polymers have high attenuation. Hence, many techniques that are used for steel testing do not work very well for fiber reinforced polymers. Here the ultrasonic guided wave technique is applied to concrete beams reinforced by glass fiber reinforced polymer bars to investigate the effect of high attenuation. This study shows that the ultrasonic guided wave testing technique has potential for both glass fiber reinforced polymer/concrete and steel/concrete interface testing.

Keywords: *guided waves, ultrasonic waves, interface testing, delamination detection, reinforced concrete testing.*

INTRODUCTION

Glass fiber reinforced polymer bars have become popular in recent years as reinforcement for concrete structures. One advantage of these bars over steel is their resistance to corrosion. Although the bars do not corrode in contact with deicing chemicals, they can deteriorate rapidly in an alkaline environment (Ehsani, 1993). Zayed (1991) showed that one type of glass fiber reinforced polymer bar subjected to a saturated solution of calcium hydroxide exhibited loss of strength due to high level of water gain. Although these results cannot be generalized, they do point out the importance of the proper material selection for both fiber and matrix for a particular application. Inadequate material selection under adverse environmental conditions may cause severe inside or outside deterioration of glass fiber reinforced polymer reinforced concrete structures. In addition, the following factors may cause deterioration of the reinforced concrete structures: poor design, poor construction, severe environments or a combination of these factors. These deteriorations may result in cracks and void formation and delamination or loss of bond between concrete and glass fiber reinforced polymer bars. Loss of bond between concrete and reinforcing material is a major concern because it results in significant weakness of the structural member.

To investigate these discontinuities, several testing techniques can be adopted. In general, nondestructive testing (NDT) is more desirable than destructive testing since the integrity of the existing structures is not compromised. Several NDT methods have been applied to civil infrastructures, such as electrochemical, impact echo, X-ray, ground penetrating radar and ultrasonic methods. Ultrasonic NDT methods have not been fully developed yet for testing of interface discontinuities in reinforced concrete, especially for the interface between glass fiber reinforced polymer bar and concrete. This is because conventional ultrasonic methods use reflection, transmission and scattering of longitudinal waves by internal discontinuities. None of these techniques are very efficient for studying the interface between glass fiber reinforced polymer and concrete (Na, 2001). Glass fiber reinforced polymer has a high attenuation rate and embedding it in concrete makes it more attenuative. Such high attenuation significantly reduces the strength of the propagating waves.

In spite of the limited applications of ultrasonic methods in interface testing of concrete, it has been shown that guided waves can be efficiently used for testing different types of discontinuities at interfaces (Pavlakovic et al., 1998; Na et al., 2002). Pavlakovic et al. (1998) used the time of flight information to identify voids at the interface between grout and steel tendons. Na et al. (2002) used inclination angle and frequency sweep techniques to test interface delamination between steel bar and concrete. Important characteristics of the guided waves are that they can propagate a long distance and they have several wave modes that are sensitive to different types of discontinuities. Thus, if one can develop well designed devices and techniques for transmitting, propagating, receiving and analyzing guided waves, interface discontinuities can be detected. It should be noted here that the range of testing distance depends on the material properties, experimental setups and so on. For example, the distance is related to the sensitivity of testing instruments and material attenuations. Pavlakovic et al. (1998) showed how to estimate the maximum test distance for their application.

This paper shows the feasibility of using guided ultrasonic waves to test the interface discontinuity in the form of delamination between the glass fiber reinforced polymer bar and concrete. Experimental and theoretical results for both glass fiber reinforced polymer and steel bars in concrete are presented and the results from these two types of reinforcing bars are compared to investigate the effect of high attenuation.

Two specimens, one reinforced with steel bars and the second one with glass fiber reinforced polymer bars, are fabricated. Each specimen contains four identical bars with different degrees of delamination, 0%, 25%, 50% and 75%, at the interface. These delaminations are fabricated artificially to idealize an interface delamination. Two different experimental setups are tried out to generate,

* Bridge Group, Arizona Department of Transportation.
† Department of Civil Engineering and Engineering Mechanics, University of Arizona, Tucson, AZ 85721; (520) 621-6573; fax (520) 621-2550; e-mail <tkundu@email.arizona.edu>.

propagate and receive guided waves through the bars and concrete. After recording the time histories for different signal frequencies, a software based on Fourier transformation produces $V(f)$ curves, or the received signal amplitude versus frequency curves. Using these curves, the degree of delamination is quantified and the modes corresponding to the peaks of the $V(f)$ curves are identified by appropriate theoretical investigation.

Theoretical studies are conducted by generating the energy velocity and attenuation dispersion curves of the specimens. The concrete and glass fiber reinforced polymer bar properties are obtained experimentally by appropriate ultrasonic testing. The specimen geometry is modeled as a solid bar embedded in an infinite concrete medium. Energy velocity dispersion curves are examined to determine which experimental points correspond to which guided wave modes. Attenuation dispersion curves are obtained to investigate the degree of attenuation for each specimen.

EXPERIMENT

Setup

For the first specimen, the diameter and length of the steel bars are 22 mm (0.9 in.) and 914 mm (36 in.), respectively. The dimensions of concrete are 250 by 250 by 610 mm (10 by 10 by 24 in.) as shown in Figure 1a. The detailed fabricating procedure for the delaminated regions is given in Na et al. (2002). The first specimen has four steel bars with 0%, 25%, 50% and 75% delaminations, respectively, as shown in Figure 1a.

For the second specimen, the nominal diameter and length of the glass fiber reinforced polymer bars are 22 mm (0.9 in.) and 914 mm (36 in.), respectively. The concrete dimensions are the same as in the previous case. To artificially create the delaminated region, polyvinyl chloride pipe was first placed and then extracted 6 h after placing the concrete into the wooden mold. The inner and outer diameters of the polyvinyl chloride pipe are 25 mm (1 in.) and 28 mm (1.1 in.), respectively. The specimen has four glass fiber reinforced polymer bars with 0%, 25%, 50% and 75% delamination at the interface (Figure 1a). In these two specimens, the smallest distance between the concrete surface and the central axis of the bars is 63.5 mm (2.5 in.).

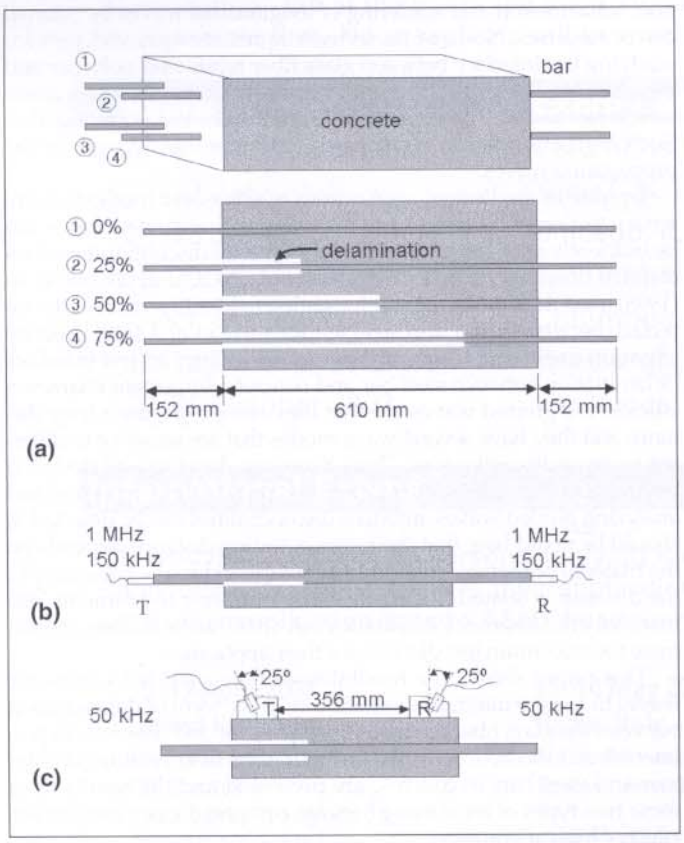

Figure 1 — Specimens and transmitter/receiver arrangements for experimental investigation: (a) reinforced concrete beam having four reinforcing bars with different degrees of delamination (the bars are either steel or glass fiber reinforced polymer); (b) transmitter and receiver in direct contact at the ends; (c) solid coupler transducer holder on concrete with 25 degree incident and reception angles.

Two experimental setups are used. One setup is for relatively low frequency transducers (10 to 500 kHz) and the second one is for relatively high frequency (> 500 kHz) transducers (Na et al., 2002). The transmitters were activated by a toneburst excitation using a commercial function generator, a gated amplifier for high frequency (> 500 kHz) excitation and an amplifier for low frequency (< 500 kHz) excitation. The excitation frequency was continuously varied from a minimum to a maximum value within the bandwidth of the transducers. The signal after its propagation through the specimens was received by a receiver and was amplified by one of two commercial amplifiers. This signal was digitized by a 40 MHz data acquisition board and the received signal was analyzed. A computer program using the Fourier transform computed the average amplitude of the signal in a given time window by continuously changing the frequency of the toneburst signal and then plotted this value against frequency to generate the $V(f)$ curves.

Figures 1b and 1c show broadband transducers and different transmitter receiver arrangements. The central frequencies of these transducers are 1 MHz, 150 kHz and 50 kHz, respectively. Diameters of the transducers are 12.7 mm (0.5 in.) for the 1 MHz transducers, 25.4 mm (1 in.) for the 150 kHz transducers, and 50.8 mm (2 in.) for the 50 kHz transducers (Na et al., 2002). Figure 1b shows a transmitter receiver arrangement that can efficiently generate longitudinal cylindrical guided waves in the glass fiber reinforced polymer bar. Figure 1c shows an arrangement with a solid coupler geometry that can hold the transducers at an inclination angle of 25 degrees. The transducer holder was placed on the concrete while for the first case (Figure 1b) the holders were placed on the bar. The distance between the centers of the transducer holders is 483 mm (19 in.). It should be noted here that the transducers are placed such that the signal striking position is approximately at the center of the transducer holder. Petroleum jelly was used as the couplant. The coupling mechanism between the transducer and the bar converts the compressional P waves generated by the ultrasonic transducers into different modes of the guided waves.

Results

The experimental results obtained from the two specimens are presented in Figures 2 through 5. For every specimen and setup, experiments were repeated eight times to study the consistency of the results. In each $V(f)$ curve, the horizontal axis shows the frequency (in kilohertz) and the vertical axis gives the received signal amplitude. Different results from multiple experiments are plotted along the third axis. Na et al. (2002) published a complete set of experimental results for the steel reinforcement (specimen one). For comparison purposes, some results (Figures 2 and 3) are presented here from that paper.

Figure 2 shows the $V(f)$ curves of specimen one generated by the transmitter/receiver arrangement of Figure 1b. Figures 2a and 2b show the $V(f)$ curves generated by the 150 kHz and 1 MHz transducers, respectively. The peak positions correspond to 100, 138, 168 and 200 kHz frequencies in Figure 2a and 1.175, 1.35, 1.525 and 1.675 MHz in Figure 2b. From these curves, one can see that the percentage of delamination has a stronger effect on the $V(f)$ curves of Figure 2a. Figure 3 shows the $V(f)$ curves of specimen one generated by the transmitter/receiver arrangement shown in Figure 1c with 50 kHz transducers. The peaks are at 53, 67, 103 and 137 kHz frequencies in Figure 3. From these curves, one can see that the percentage of delamination has a strong effect on the $V(f)$ curves of Figure 3 also. Na et al. (2002) have shown that for the transmitter/receiver arrangement shown in Figure 1c, the experimental results depend on the distance between the surface of the concrete and the delamination. However, when the bar ends are not accessible, then the transducer/receiver arrangement shown in Figure 1c can be used.

The $V(f)$ curves for specimen two generated by the transducer arrangements given in Figures 1b and 1c are shown in Figures 4

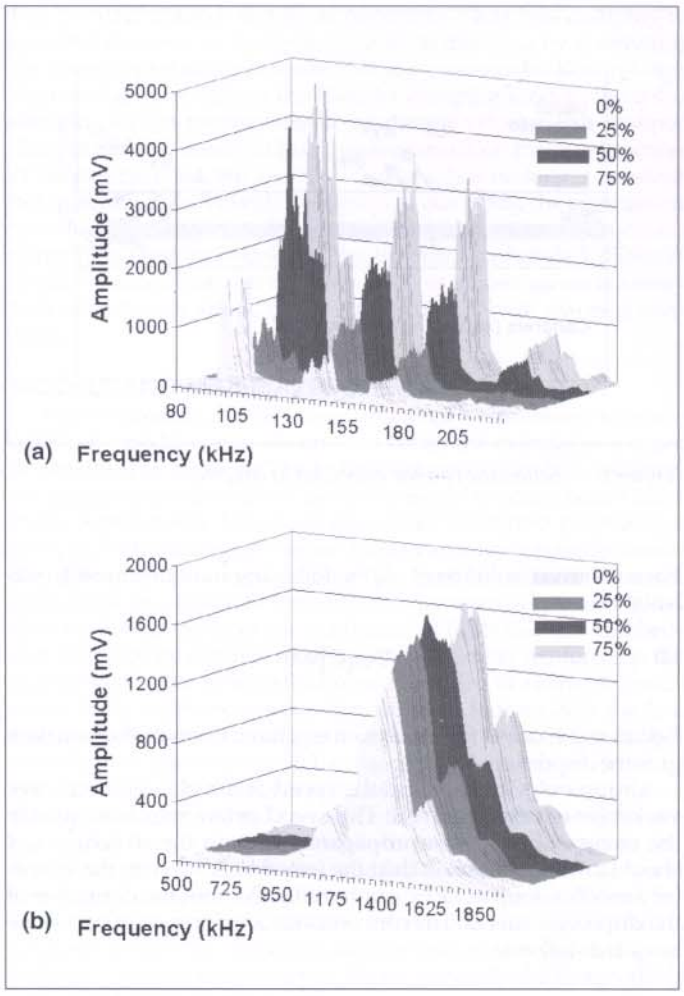

Figure 2 — V(f) curves of specimen one using transmitter/receiver arrangement as shown in Figure 1b. The transducer frequencies are: (a) 150 kHz; (b) 1 MHz.

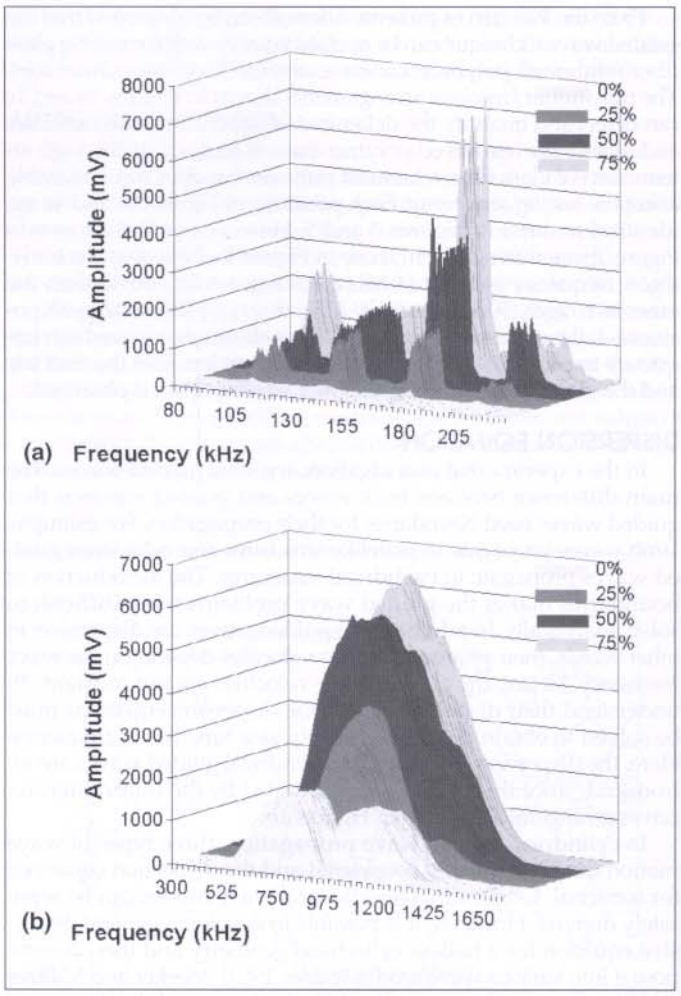

Figure 4 — V(f) curves of specimen two using transmitter/receiver arrangement as shown in Figure 1b. The frequencies of transmitters are: (a) 150 kHz; (b) 1 MHz.

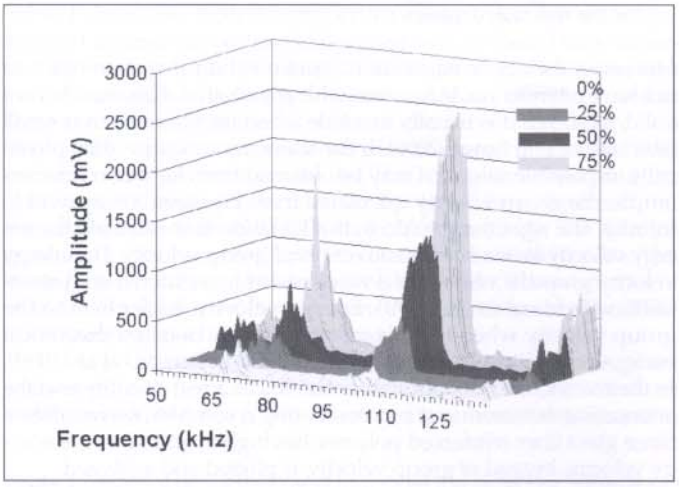

Figure 3 — V(f) curves of specimen one using transmitter/receiver arrangement as shown in Figure 1c.

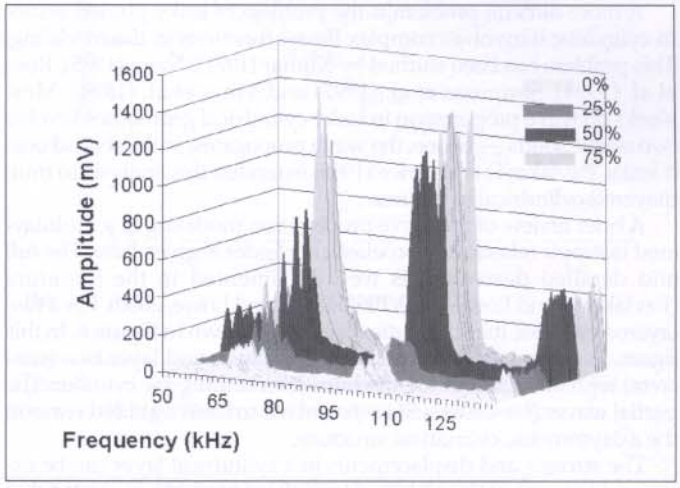

Figure 5 — V(f) curves of specimen two using transmitter/receiver arrangement as shown in Figure 1c.

and 5, respectively. Figure 4 shows the *V(f)* curves of specimen two generated by the transmitter/receiver arrangement of Figure 1b. Figure 4a shows the *V(f)* curves when 150 kHz transducers are used and the *V(f)* curves of Figure 4b are generated by the 1 MHz transducers. The peak positions are 100, 138, 168 and 203 kHz in Figure 4a and 875 kHz in Figure 4b. From these curves, one can see that the percentage of delamination has a stronger effect on the *V(f)* curves of Figure 4a. However, only one peak in Figure 4a shows noticeable monotonic increase of the peak value with the increase in the delamination length. The peak in Figure 4b is broader and also sensitive to the interface delamination length. Figure 5 shows the *V(f)* curves of specimen two generated by the transmitter/receiver arrangement shown in Figure 1c with 50 kHz transducers. The peak positions are 53, 67, 103 and 137 kHz in Figure 5. From these curves, one can see that the percentage of delamination has strong effects on the peaks of the *V(f)* curves of Figure 5 also.

From the $V(f)$ curves presented here, it can be concluded that the guided wave technique can be applied equally well for testing glass fiber reinforced polymer/concrete and steel/concrete interfaces. The transmitter/receiver arrangements shown in Figures 1b and 1c can detect and quantify the delaminated regions for both steel bars and glass fiber reinforced polymer bars. It seems that the high attenuation of glass fiber reinforced polymer bar does not noticeably affect the testing sensitivity. Peak positions of Figures 2a and 4a are identical to those in Figures 3 and 5. However, peak locations in Figure 2b are different from those in Figure 4b. Note that the transducer frequency is larger (1 MHz) for Figures 2b and 4b than the other two cases (50 kHz and 150 kHz) that gave the same peak positions in the corresponding figures. This shows that when high frequency transducers are used, some difference between the steel bar and the glass fiber reinforced polymer bar responses is observed.

DISPERSION EQUATION

In the experimental investigation, we used guided waves. The main difference between bulk waves and guided waves is that guided waves need boundaries for their propagation. For example, lamb waves propagate in platelike structures and cylindrical guided waves propagate in cylindrical structures. The introduction of boundaries makes the guided wave problems more difficult to solve analytically. In addition, the guided waves are dispersive; in other words, their phase and group velocities depend on the wave frequency. Hence, the guided wave velocities are not constant. To understand their dispersive nature the dispersion equations must be solved to obtain the phase velocity as a function of frequency. Here, the dispersion equations for cylindrical guided waves are introduced, since these waves are generated by the transmitter/receiver arrangements shown in Figures 1b.

In cylindrical guided wave propagation, three types of wave motion can be separately considered and the dispersion equations for torsional, longitudinal and flexural wave modes can be separately derived. However, it is possible to develop a general dispersive equation for a hollow cylindrical geometry and then decompose it into various wave modes (Gazis, 1959). Meeker and Meitzer (1972), following the approach of Gazis, developed the dispersion equations for a solid cylinder. Detailed information on this technique can be found in Achenbach (1984), Graff (1991), Kolsky (1963), Meitzler (1965), Mindlin and McNiven (1960), Onoe et al. (1962), Pao (1962), Pao and Mindlin (1960) and Rose (1999).

A more difficult problem is the problem of leaky guided waves in cylinders; it involves complex Bessel functions in the modeling. This problem has been studied by Kumar (1971), Nagy (1995), Rose et al. (1994), Simmons et al. (1992) and Vines et al. (1994). Most works on wave propagation in leaky cylindrical geometries involve two elastic solids — in one, the wave propagates; in the second one, it leaks. Pavlakovic and Lowe (1999) extended this analysis to multilayered cylindrical structures.

A brief review of the wave propagation modeling in a multilayered isotropic (elastic or viscoelastic) cylinder is given here. The full and detailed derivation is well documented in the literature (Pavlakovic and Lowe, 1999; Pavlakovic and Lowe, 2000). For a two layered cylinder, the schematic diagram is shown in Figure 6. In this figure, layer one (bar) represents a finite layer and layer two (concrete) represents an infinite medium surrounding the cylinder. The partial waves (L+–, SV+–, SH+–) combine to form a guided wave in the axisymmetric cylindrical structure.

The stresses and displacements in a cylindrical layer can be expressed in terms of the amplitudes of all waves that can exist in that layer. Then the continuity of stresses and displacements at the common boundaries of adjacent layers as well as boundary conditions at the outermost and innermost surfaces (or top and bottom surfaces for multilayered plates) are satisfied to obtain one large global matrix equation (Pavlakovic and Lowe, 2000).

$$[G]\{A\} = 0 \tag{1}$$

where

$[G]$ = the global matrix

$\{A\}$ = a vector of partial wave amplitudes.

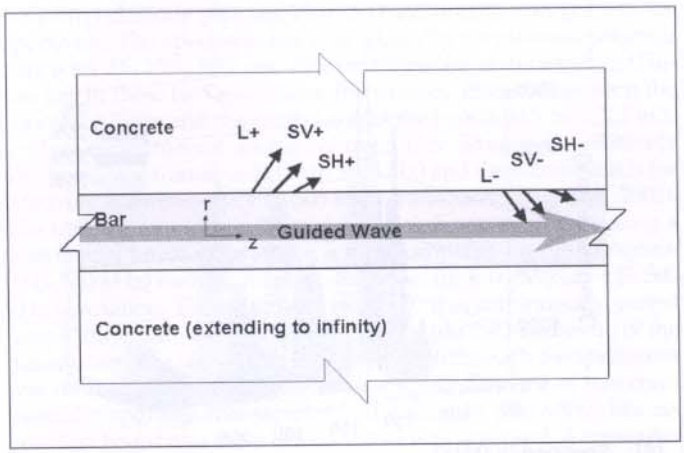

Figure 6 — Schematic of a bar embedded in concrete.

For a nontrivial solution of $\{A\}$ the following condition must be satisfied:

$$\mathrm{Det}[G] = 0 \tag{2}$$

Equation 2 is called the dispersion equation. Roots of this equation give the dispersion curves.

Group velocity indicates the speed at which a guided wave packet (or envelope) travels. This speed determines how quickly the energy of the wave propagates through the structure and should always be smaller than the fastest bulk wave in the system (or model). Group velocity can be obtained from the derivative of the dispersion curves. The conventional definition of group velocity v_{gr} is as follows:

$$v_{gr} = \frac{\partial \omega}{\partial k} \tag{3}$$

where

ω = the angular velocity

k = the real wave number.

However, the above equation is strictly valid for systems that do not have attenuation. In systems with attenuation, Equation 3 is not valid, although it is usually accurate when the attenuation is small (Pavlakovic and Lowe, 2000). If the attenuation is large, then physically impossible solutions may be obtained from Equation 3; for example, the group velocity calculated from Equation 3 may tend to infinity. The right thing to do in this situation is to calculate the energy velocity instead of the conventional group velocity. The energy velocity gives the velocity of a wave packet in a material with attenuation (Bernard et al., 1999). Energy velocity is identical to the group velocity when there is no attenuation. Detailed theoretical background of energy velocity can be found in Bernard et al. (1999). In their work, the frequency is considered as a real quantity and the attenuation is introduced by considering a complex wavenumber. Since glass fiber reinforced polymer has high attenuation, the energy velocity, instead of group velocity, is plotted and analyzed.

Attenuation is an important parameter that has a strong effect on the guided wave propagation characteristics in a given system (Na and Kundu, 2002). The attenuation value determines how the wave strength decays when it propagates in a system. Whenever damping materials are present in the system (or model), there is energy loss associated with it. There are several ways to express the damping property of each layer in a given system: hysteretic structural damping; hysteretic damping; and Kelvin-Voigt viscous damping. Hysteretic structural damping defines a damping loss, which is a constant per wavelength traveled. The units of this damping can be nepers per wavelength or decibel per wavelength. Hysteretic damping enables the bulk attenuation to be defined as a

loss per unit distance at a given frequency. Thus, this damping is basically the same as hysteretic structural damping by converting the loss per unit distance to the loss per wavelength. Kelvin-Voigt viscous damping defines the dashpot damping model where the damping force is proportional to the particle velocity. This dashpot damping model results in bulk wave attenuation that is a function of frequency. Thus, the loss per wavelength is no longer constant but increases linearly with frequency. In our study, the attenuation of bulk waves is constant, which means the hysteretic structural damping is used for calculating the attenuation of guided waves. It should be noted here that the attenuation of guided waves is a function of frequency although the attenuation of bulk waves is constant.

MODELS AND MATERIAL PROPERTIES

For constructing the dispersion equation, it is necessary to mathematically model our specimens and obtain the material properties of each layer of the model. Four different models can be considered for getting dispersion curves of the reinforced concrete beams used in the experiments. These are: glass fiber reinforced polymer (or steel) bar of finite diameter embedded in an infinite concrete medium; glass fiber reinforced polymer (or steel) bar of finite diameter embedded in a concrete bar of finite diameter in vacuum; glass fiber reinforced polymer (or steel) plate of finite thickness embedded in an infinite concrete medium; and glass fiber reinforced polymer (or steel) plate of finite thickness embedded in a concrete medium of finite width in vacuum. Among these four models, the first two might be better suited for our specimens since the glass fiber reinforced polymer (or steel) bar has a cylindrical shape. In addition, from the computational point of view, the first model is more efficient than the second one since the first model has only one solid/solid interface condition while the second model has two different conditions: for example, solid/solid interface condition and stress free boundary condition (or solid vacuum condition). Increasing the number of layers and interface/boundary conditions adversely affects the computational time and accuracy and makes it difficult to get dispersion curves. That is why only the first model is considered in our analysis.

To determine the material properties of the concrete beams and glass fiber reinforced polymer bars, ultrasonic tests were conducted (Na, 2001). Longitudinal and shear wave transducers of 1 MHz central frequency were used to measure velocities and attenuations. Table 1 shows the material properties. Here, λ denotes the wavelength. Concrete properties of specimen two are found to be different from those of specimen one. This is because specimen one was cast several months before specimen two. Hence, concretes used in these two sets are not identical. A velocity measuring device was also used to measure the longitudinal wave speed in concrete. Two measurements gave similar results. The Young's modulus and the Poisson's ratio of glass fiber reinforced polymer bars, obtained from the ultrasonic test, are 40.28 GPa and 0.25, respectively. The Young's modulus value provided by the manufacturer is 40.81 GPa. The manufacturer did not provide the Poisson's ratio. The properties of steel are obtained from the literature (Pavlakovic and Lowe, 2000) and the attenuation in steel is ignored.

It should be noted here that the relative attenuation is measured following the technique outlined in Krautkrämer and Krautkrämer (1983) and *ASTM E-664* (1993). Absolute measurement of attenuation is very difficult because the echo amplitude depends not only on the material attenuation but also on a number of other influencing factors (Papadakis, 1999; Krautkrämer and Krautkrämer, 1983).

MODE IDENTIFICATION

By solving the dispersion equation, the energy velocity and attenuation dispersion curves are obtained. Figure 7 shows the energy velocity dispersion curves for specimens one and two. Figure 8 shows the attenuation dispersion curves for the two specimens. The main reason why the dispersion curves of the two specimens are different is that the glass fiber reinforced polymer bar has higher attenuation than concrete while the steel has negligible attenuation. Another reason is the acoustic impedance mismatch between the bar and the concrete. Pavlakovic et al. (2001) showed that the acoustic impedance mismatch between the steel bar (with small attenuation) and the imbedding media affects the minimum values of attenuation; the minimum attenuation value increases as the impedance of the imbedding material increases.

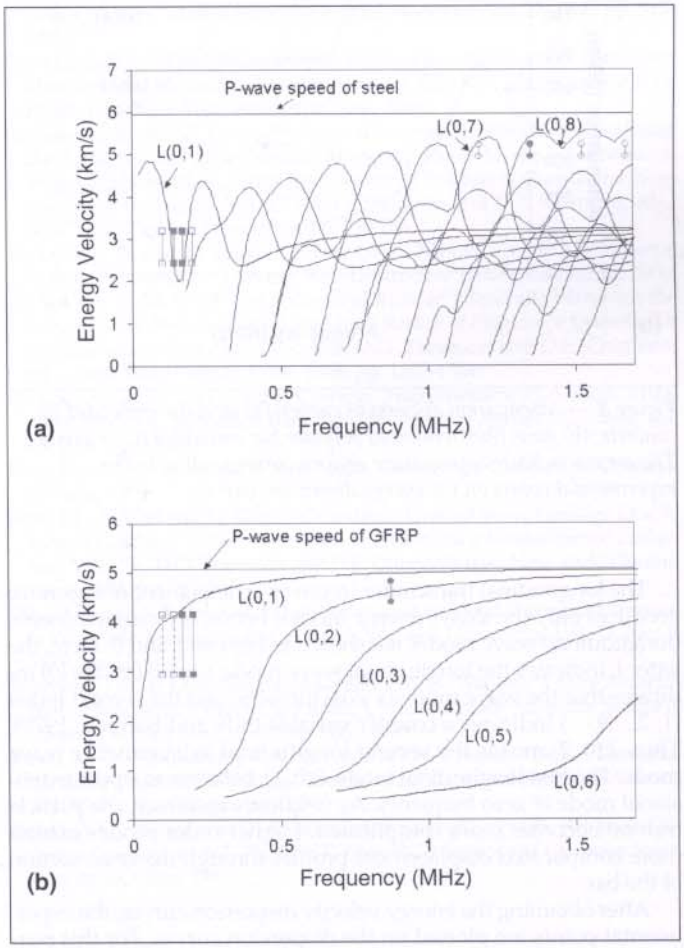

Figure 7 — Energy velocity dispersion curves: (a) steel embedded in concrete; (b) glass fiber reinforced polymer embedded in concrete.

Table 1 Material properties used to model the steel bar, glass fiber reinforced polymer bar and concrete for two specimens

Specimen	Material	Density	P-wave Velocity	S-wave Velocity	P-wave Attenuation	S-wave Attenuation
1	Steel	7932 kg/m³ (495 lb/ft³)	5960 m/s (19 600 ft/s)	3260 m/s (10 700 ft/s)	0 Np/λ	0 Np/λ
	Concrete	2120 kg/m³ (132 lb/ft³)	3745 m/s (12 300 ft/s)	2304 m/s (7560 ft/s)	0.264 Np/λ	0.311 Np/λ
2	Glass fiber reinforced polymer	1865 kg/m³ (116 lb/ft³)	5065 m/s (16 600 ft/s)	2946 m/s (9670 ft/s)	0.049 Np/λ	0.479 Np/λ
	Concrete	2040 kg/m³ (127 lb/ft³)	3721 m/s (12 200 ft/s)	2387 m/s (7830 ft/s)	0.177 Np/λ	0.286 Np/λ

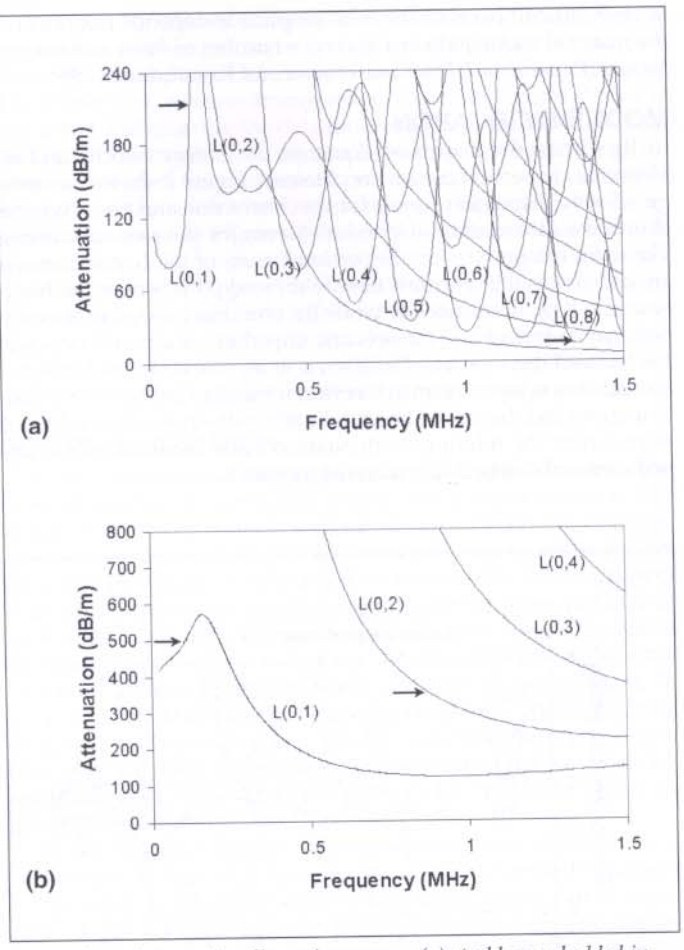

Figure 8 — Attenuation dispersion curves: (a) steel bar embedded in concrete; (b) glass fiber reinforced polymer bar embedded in concrete. The arrows indicate approximate regions corresponding to the experimental points on the energy dispersion curves.

The longitudinal transmitter/receiver arrangement of Figure 1b produces only the axisymmetric modes; hence, only axisymmetric (longitudinal) wave modes are shown in Figures 7 and 8. Here, the letter L indicates the longitudinal wave mode; the first index (0) indicates that the wave mode is axisymmetric and the second index (1, 2,…9,…) indicates a counter variable (Silk and Bainton, 1979). Thus, $L(0, 2)$ means the second longitudinal axisymmetric wave mode. The first longitudinal mode, $L(0, 1)$, behaves as a pure extensional mode at zero frequency. As frequency increases, the particle motion becomes more complicated. Higher order modes exhibit more complicated displacement profiles through the cross section of the bar.

After obtaining the energy velocity dispersion curves, the experimental points are plotted on the dispersion curves. For this purpose, the $V(f)$ curves of Figures 2 and 4 are used to find the wave mode frequencies and the gate control information used for obtaining the energy velocities. The procedure for obtaining phase velocity is explained in Na et al. (2002) and Kundu et al. (1996). For inclined incidence, Snell's law can be used for obtaining the phase velocity and mode identification. However, for the zero incident angle of the transmitter, as shown in Figure 1b, the Snell's law technique is not useful. That is why the energy velocity obtained from the gate control data is used for the mode identification.

To calculate the energy velocity, one should understand the gate control. In the experimental setup, one can control the gate (or receiving time window) position and gate width using computer software. By controlling the gate, one captures the received signal over a certain time window. The gate position and width are adjusted to obtain the clear peaks of $V(f)$ curves. The energy velocity range is calculated from the following equations:

$$v_{gr1} = \frac{l}{t_1} \tag{4}$$

$$v_{gr2} = \frac{l}{t_2} \tag{5}$$

$$t_1 = t_0 - \frac{dt}{2} \tag{6}$$

$$t_2 = t_0 + \frac{dt}{2} \tag{7}$$

where

t_0 = the gate (or time) position

dt = the gate (or time) width

l = the distance between the transmitter and the receiver.

The v_{gr1} and v_{gr2} values are the maximum and minimum values of the energy velocity. These values are used to plot the energy velocity range on the energy velocity dispersion curves. Attenuation measurements are also useful for mode identification but it is not easy to accurately measure the attenuation of the guided waves and it is not considered here.

Since we consider only axisymmetric (longitudinal) wave modes for our wave mode identification, the $V(f)$ curves of Figures 2 and 4 are used to obtain the wave mode frequencies. In Figure 2a, the frequencies corresponding to the four peaks are 100, 138, 168 and 200 kHz and the frequencies corresponding to the four peaks in Figure 2b are 1.175, 1.35, 1.525 and 1.675 MHz. The calculated energy velocity range is 2.4 to 3.2 km/s (1.5 to 2 mi/s) for Figure 2a and 4.9 to 5.2 km/s (3 to 3.2 mi/s) for Figure 2b. These experimental points are plotted on Figure 7a by using squares and circles. Here, the solid squares and circles represent strong and consistent peaks of Figure 2 and are connected by continuous lines. The smaller open squares and circles represent weak and inconsistent peaks of Figure 2 and are connected by dashed lines. Continuous and dashed lines connect the upper and lower limits of the energy velocity values at the frequencies obtained from the $V(f)$ curves.

In Figure 4a, the frequencies corresponding to the four peaks are 100, 138, 168 and 203 kHz and the frequency corresponding to the single peak in Figure 4b is 875 kHz. The calculated energy velocity range is 2.9 to 4.1 km/s (1.8 to 2.6 mi/s) for Figure 4a and 4.4 to 4.8 km/s (2.7 to 3 mi/s) for Figure 4b. These experimental points are plotted on Figure 7b by using squares and circles. Here, the solid square and solid circle represent strong and consistent peaks of Figure 4 and are connected by continuous lines. The open squares represent weak and inconsistent peaks of Figure 4 and are connected by dashed lines.

For specimen one, the longitudinal wave modes corresponding to the peak positions are likely $L(0, 1)$, $L(0, 7)$, and $L(0, 8)$ as shown in Figure 7a, while for specimen two the longitudinal wave modes are possibly $L(0, 1)$ and $L(0, 2)$ as shown in Figure 7b. In the low frequency range, the peak positions correspond to the $L(0, 1)$ mode for both specimens. However, at high frequencies the propagating wave modes are different for the two specimens. Figure 8 shows the attenuation dispersion curves for the two specimens. The arrows indicate approximate regions corresponding to the experimental points on the energy dispersion curves. The attenuation of glass fiber reinforced polymer embedded in concrete (Figure 8b) is much higher than that of steel embedded in concrete (Figure 8a). Although the attenuation of the concrete used in specimen one is larger than that in specimen two, overall attenuation of the specimen is much greater for specimen two. Clearly, the attenuation of glass fiber reinforced polymer bar dominates in computing the attenuation of the guided waves. This analysis helps us identify the right modes for efficiently detecting the delamination at the interface between the concrete and reinforcing bars and figure out the effect of attenuation on the guided wave propagation.

CONCLUSION

Ultrasonic guided waves are proposed for testing for delamination at the interface between concrete and the reinforcing bars made of glass fiber reinforced polymer and steel. Two transmitter/receiver arrangements are tried out to propagate the guided waves through the specimens. *V(f)* curves, frequency versus signal amplitude curves, obtained from the experiments, are analyzed for the delamination detection and quantification. For wave mode identification, the specimens are modeled as the cylindrical bar of a finite diameter embedded in an infinite concrete medium. The material properties in each layer are obtained from ultrasonic testing and some of those values are verified by alternative measurements. Energy velocity and attenuation dispersion curves are obtained and the peak positions of the *V(f)* curves are plotted on the velocity dispersion curves. It is found that the ultrasonic guided wave technique has potential for interface testing. This study can be used for selecting proper wave modes and frequencies for interface testing.

ACKNOWLEDGMENTS

This research was supported by the National Science Foundation (grants CMS-9800345 and 9901221). The authors appreciate the support of Hughes Brothers, Inc., Nebraska, for donating the glass fiber reinforced polymer reinforcement bars used in the experiments.

REFERENCES

ASTM, *ASTM E-664: Standard Practice for the Measurement of the Apparent Attenuation of Longitudinal Ultrasonic Waves by Immersion Method*, Philadelphia, American Society for Testing and Materials, 1993.

Achenbach, J.D., *Wave Propagation in Elastic Solids*, New York, Elsevier, 1984.

Bernard, A., M. Deschamps and M. Lowe, "Energy Velocity and Group Velocity for Guided Waves Propagating within an Absorbing or Non-absorbing Plate in Vacuum," *Review of Progress in Quantitative Nondestructive Evaluation*, Vol. 18A, D.O. Thomson and D.E. Chimenti, eds., New York, Plenum Press, 1999, pp. 183-190.

Ehsani, M., "Glass-fiber Reinforcing Bars," *Alternative Materials for the Reinforcement and Prestressing of Concrete*, J.L. Clarke, ed., London, Blackie Academic & Professional, 1993, pp. 34-54.

Gazis, D.C., "Three-dimensional Investigation of the Propagation of Waves in Hollow Circular Cylinders, I. Analytical Foundation," *Journal of the Acoustical Society of America*, Vol. 31, No. 5, 1959, pp. 568-573.

Graff, K.F., *Wave Motion in Elastic Solids*, New York, Dover Publications, 1991.

Kolsky, H., *Stress Waves in Solids*, New York, Dover Publications, 1963.

Krautkrämer, J. and H. Krautkrämer, *Ultrasonic Testing of Materials*, third edition, New York, Spring-Verlag, 1983.

Kumar, R., "Flexural Vibrations of Fluid-filled Circular Cylindrical Shells," *Acoustica*, Vol. 24, 1971, pp. 137-146.

Kundu, T., K. Maslov, P. Karpur, T.E. Matikas and P.D. Nicolaou, "A Lamb Wave Scanning Approach for the Mapping of Defects in [0/90] Titanium Matrix Composites," *Ultrasonics*, Vol. 34, 1996, pp. 43-49.

Meeker, T.R. and A.H. Meitzler, "Guided Wave Propagation in Elongated Cylinder and Plates," *Physical Acoustic Principles and Methods*, Vol. 1A, W.P. Mason and R.N. Thurston, eds., New York, Academic Press, 1972, pp. 111-167.

Meitzler, A.H., "Backward-wave Transmission of Stress Pulses in Elastic Cylinders and Plates," *Journal of the Acoustical Society of America*, Vol. 38, No. 5, 1965, pp. 835-842.

Mindlin, R.D. and H.D. McNiven, "Axially Symmetric Waves in Elastic Rods," *Journal of Applied Mechanics*, Vol. 27, 1960, pp. 145-151.

Na, W.B., "Nondestructive Evaluation of Bar-concrete Interface in Reinforced Concrete Structures," PhD dissertation, Department of Civil Engineering and Engineering Mechanics, University of Arizona, 2001.

Na, W.B. and T. Kundu, "Wave Attenuation in Pipes and Its Application in Determining Axial Spacing of Monitoring Sensors," *Materials Evaluation*, Vol. 60, 2002, pp. 635-644.

Na, W.B., T. Kundu and M.R. Ehsani, "Ultrasonic Guided Waves for Steel Bar Concrete Interface Testing," *Materials Evaluation*, Vol. 60, 2002, pp. 437-444.

Nagy, P.B., "Longitudinal Guided Wave Propagation in a Transversely Isotropic Rod Immersed in Fluid," *Journal of the Acoustical Society of America*, Vol. 98, No. 1, 1995, pp. 454-457.

Onoe, M, H.D. McNiven and R.D. Mindlin, "Dispersion of Axially Symmetric Waves in Elastic Solids," *ASME Journal of Applied Mechanics*, Vol. 29, 1962, pp. 729-734.

Pao, Y.H., "The Dispersion of Flexural Waves in an Elastic, Circular Cylinder: Part 2," *ASME Journal of Applied Mechanics*, Vol. 29, 1962, pp. 61-64.

Pao, Y.H. and R.D. Mindlin, "Dispersion of Flexural Waves in an Elastic, Circular Cylinder," *ASME Journal of Applied Mechanics*, Vol. 27, 1960, pp. 513-520.

Papadakis, E.P., "The Measurement of Ultrasonic Attenuation: Ultrasonic Measurement Methods," *Physical Acoustics XIX*, R.N. Thurston and A.D. Pierce, eds., New York, Academic Press, 1999.

Pavlakovic, B. and M. Lowe, "A General Purpose Approach to Calculating the Longitudinal and Flexural Modes of Multi-layered, Embedded, Transversely Isotropic Cylinders," *Review of Progress in Quantitative Nondestructive Evaluation*, Vol. 18A, D.O. Thomson and D.E. Chimenti, eds., New York, Plenum Press, 1999, pp. 239-246.

Pavlakovic, B. and M. Lowe, *Disperse User's Manual Version 2.0*, Imperial College, University of London, Non-Destructive Testing Laboratory, 2000.

Pavlakovic, B., M. Lowe and P. Cawley, "Guided Ultrasonic Waves for the Inspection of Post-tensioned Bridges," *Review of Progress in Quantitative Nondestructive Evaluation*, Vol. 17B, D.O. Thomson and D.E. Chimenti, eds., New York, Plenum Press, 1998, pp. 1557-1564.

Pavlakovic, B., M. Lowe and P. Cawley, "High-frequency Low-loss Ultrasonic Modes in Imbedded Bars," *ASME Journal of Applied Mechanics*, Vol. 68, 2001, pp. 67-75.

Rose, J.L., *Ultrasonic Waves in Solid Media*, Cambridge, Cambridge University Press, 1999.

Rose, J.L., Y. Cho and J.J. Ditri, "Cylindrical Guided Wave Leakage Due to Liquid Loading," *Review of Progress in Quantitative Nondestructive Evaluation*, Vol. 13A, D.O. Thomson and D.E. Chimenti, eds., New York, Plenum Press, 1994, pp. 259-266.

Silk, M.G. and K.F. Bainton, "The Propagation in Metal Tubing of Ultrasonic Wave Modes Equivalent to Lamb Waves," *Ultrasonics*, Vol. 17, No. 1, 1979, pp. 11-19.

Simmons, J.A., E. Drescher-Krasicka and H.N.G. Wadley, "Leaky Axisymmetric Modes in Infinite Clad Rods, I," *Journal of the Acoustical Society of America*, Vol. 92, No. 2, 1992, pp. 1061-1090.

Vines, M., Y. Tshukahara, C.K. Jen and J.D.N. Cheeke, "Leaky Torsional Modes in Infinite Clad Rods," *Journal of the Acoustical Society of America*, Vol. 95, No. 2, 1994, pp. 701-707.

Zayed, A.M., "Deterioration Assessment of Fiber-glass Plastic Rebars in Different Environments," *The NACE Annual Conference and Corrosion Show*, Cincinnati, Ohio, 1991.